Visualization of Fracture Intersections from 3D X-ray Imaging

Madelyn Sumner
Purdue University, West Lafayette, Indiana, USA

Laura J. Pyrak-Nolte
Purdue University, West Lafayette, Indiana, USA

ABSTRACT: Though fracture intersections control the connectivity of a fracture network, few studies have examined the deformation of intersections. A laboratory study was performed to examine the effect of an applied stress on a fracture network and the intersection geometry. 3D printing was used to create 2 orthogonal intersecting fractures with either a "+" or "x" orientation relative to an applied vertical load. 3D X-ray microscopy was used to image the fracture network. For the "+" orientation, the network connectivity was maintained by the vertical fracture that did not deform significantly under load. However, for the "x" orientation, the void volume and connectivity between the two fractures decreased significantly and almost ceased to exist at the highest load as the topology transitioned from "X" to "Z" to "V". Hydro-mechanical modeling of fracture networks may need to account for changes in intersection connectivity from perturbations in stress.

Keywords: Fracture networks, fracture intersections, apertures, stress, imaging.

1 INTRODUCTION

The sustainable production of conventional, unconventional, and geothermal energy resources often relies on the injection and withdrawal of fluids through natural and induced fracture networks. The three-dimensional connectivity of flow paths through fracture networks depends crucially on fracture intersections. The geometry of intersections depends on a multiplicity of factors that range from the original creation of the fractures relative to bedding planes and rock anisotropy to the orientation of the stress and pressure fields during production to erosion and precipitation from geochemical alteration of the void space. Most past research has focused on the mechanical and hydraulic behavior of single fractures (e.g., Brown & Scholz, 1987; Cook, 1992; Pyrak-Nolte & Nolte, 2016). Transitioning from an individual fracture to a 3D fracture network increases the complexity of a fracture system by introducing fracture intersections. Laboratory studies on fracture networks have focused on fluid flow paths through fractures network (e.g., Hull, 1986; Johnson & Brown, 2001), 3D network geometry (Montemagno & Pyrak-Nolte, 1999) as well as 2D imaging of the deformation of networks under stress (e.g. Frash et al., 2016).

In this paper, results from a laboratory study on the geometry of 3D fracture intersections are presented that examined two questions: (1) What happens to the geometry of an intersection and the topology of a network when they reside inside the same network topology but have a different orientation relative to an applied stress field (Figure 1c&d)? and (2) How do spatial correlations in the fracture aperture distribution affect the geometry of the intersection between two orthogonal fractures (Figure 1a&b)?

2   EXPERIMENTAL APPROACH

2.1   Sample Preparation

3D printing was used to fabricate fracture network samples ($\sim$ 6 x 6 x 6 mm^3) composed of two orthogonal fractures. A Formlabs Form 3 printer was used to print (layer thickness $\sim$ 25 μm) either four assembled triangular or rectangular prisms ($\sim$ 3 x 3 x 6 mm^3 each) to create either an 'x' or "+" (Figure 1c&d) when placed perpendicularly to an applied vertical load. All samples were printed vertically (i.e., the long axis of the prism was perpendicular to the printed layer, Figure 1c&d) to ensure the same material response among samples. The surface roughness of the individual fracture planes was either random (Figure 1a) or spatially correlated (Figure 1b) and was generated using a stratified percolation approach (Nolte & Pyrak-Nolte, 1991). The spatial correlations in the aperture distribution were controlled by the surface roughness. For each independent fracture network, opposing fracture surfaces within the network had the same roughness with opposite curvature, i.e. the surfaces were not mated. The apertures in each pattern ranged from 0 (contact area or apertures less than imaging resolution) to 450 micrometers. Here, samples with a random surface roughness are referred to as "uncorrelated", while the samples with spatially correlated surface roughness are referred to as "correlated".
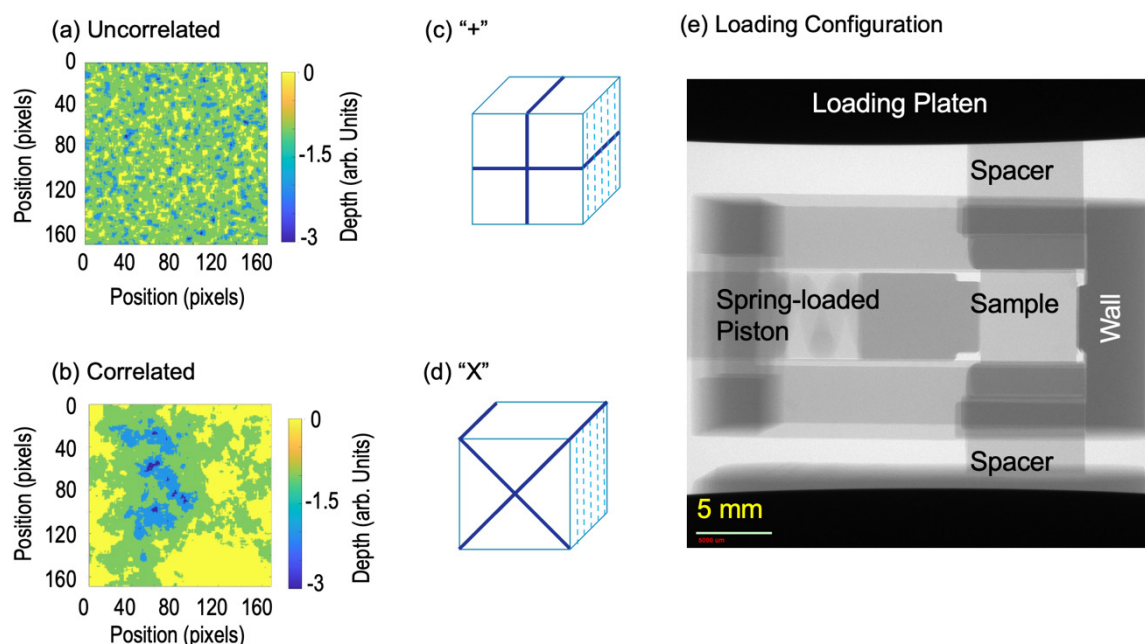

Figure 1. Images of the (a) uncorrelated and (b) correlated surface roughness (increasing depth into the page from yellow to blue, arbitrary units). (c) "+" and (d) "x" orientations relative to an applied vertical load (light blue dashed indicate orientation of 3D printing layers – note not drawn to scale). (e) The loading configuration with the custom-frame for lateral confinement. When placed in the (e) set-up the samples are oriented as shown in (c) & (d).

2.2 Sample Confinement and Loading

A normal load was applied to a sample using a Deben CT5000 in-situ uniaxial loading device. A loading rate of 0.1 mm/minute was used. For each load (25 N and 200 N), after the load was attained the displacement was held constant and the sample was allowed to equilibrate for 30 minutes prior to initiating the 3D X-ray scans. A custom loading frame (Figure 1e) was 3D printed on the same FormLabs printer with the same settings to provide weak lateral confinement (~5N) perpendicular to the normal load along one axis (Figure 1e). The normal was applied to the top and bottom faces of the sample (Figure 1c&d). The weak lateral confinement (to left and right faces in Figure 1c&d) was provided by a spring with a spring constant of roughly 10 N/mm. The sample was allowed to expand freely in the 3rd orthogonal direction (out of the page in Figures 1c,d,e). Santos et al. (2022) performed a stress analysis of this loading configuration using a microscale mechanical model based on the numerical manifold method, NNM (Hu and Rutqvist, 2020). From simulations, the normal stress was relatively uniform across a solid sample with shear stress concentrations at the contacts between the Deben's platens and loading spacers, and between the spacers and the sample. The frame was updated with a protruding wall to center the sample to prevent preferential closure from bending that was observed in the simulations.

2.3 3D X-ray Microscopy & Analysis

3D imaging of the fracture network geometry under load was performed using a Zeiss Xradia 510 Versa 3D X-ray microscope. The settings used for 3D imaging of the samples were 80 kV and 7 W X-rays with a 0.4x magnification, and source and detector distances of 84 mm and 300 mm, respectively. A 3.5 sec exposure time with bin 2 was used for each of the 2401 projections. This yielded a voxel edge length of ~15μm.

Dragonfly ORS was used to reconstruct the 2D Xray projections of each sample into a 3D fracture network and to create segmented 2D images of the fracture network void geometry. The 2D images were taken perpendicular to the long axis of the intersection. A custom code in IDL® was written to identify the intersection region in the exported images based on a method that used the distance from the center of an intersection to the fracture walls to calculate a potential. The center of the intersection was chosen manually for the first and last frames, and then linear interpolation was used to track the intersection frame-to-frame. For each image, the matrix was set to 0 and the void space to 1. A thinning function was applied to each image after using a Sobel edge detector function to find the edges of the fractures. The location of each edge pixel was used to calculate the distance between the center and the edges. These distances were used to calculate the potential. Pixels that were less than a selected potential threshold were labeled as intersection pixels. Then a convex hull approach coupled with an ellipse fitting procedure was applied to quantify the geometry of the intersection.

3 RESULTS & DISCUSSION

Outcrops and boreholes present 2D views of fracture networks though fracture networks are intrinsically 3D. The topology of two intersecting fractures based on a 2D view, are often labeled as "X", "T", "V" and "Z" topologies (Bai & Pollard, 2000; Sanderson & Nixon, 2015; Laubach et al., 2019). In our study, the "X" topology was selected which consists of 2 orthogonal fractures forming 1 intersection, with either a "+" or "x" orientation relative to an applied normal stress (Figure 1). Figures 2 & 3 provide a visual comparison of the effect of network orientation relative to stress on the topology and connectivity of the fracture network. For the "+" orientation, the horizontal fracture closed as the load was increased from 25 N to 200 N. This is observed from the increase in the number of white regions in Figure 2(a-d) that represent regions that are smaller than the voxel edge length and/or contact area. The connectivity of the fracture network was maintained by the vertical fracture that did not deform significantly under load. The topology transitioned at most from a "+" to "T" topology (e.g., "|—") orientation along portions of the network where voids in the horizontal fracture immediately adjacent to the intersection closed (Figure 2g).
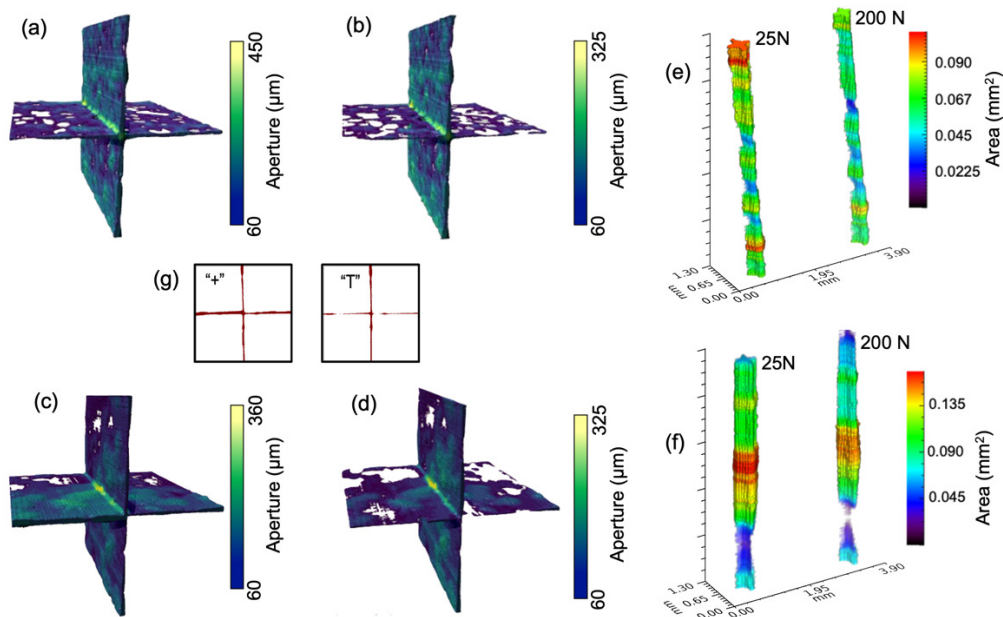
Figure 2. 3D reconstruction of the apertures for the "+" fracture networks with (a&b) random distribution of apertures under (a) 25 N and (b) 200 N, and with (c&d) a spatially correlated aperture distribution under (c) 25 N and (d) 200 N. The geometry of the intersection for loads 25 N and 200 N for the (e) random and (f) spatially correlated aperture distributions. (g) 2D images of same intersection location at 25 N and 200 N illustrating the transition from a "+" to a "T" topology.
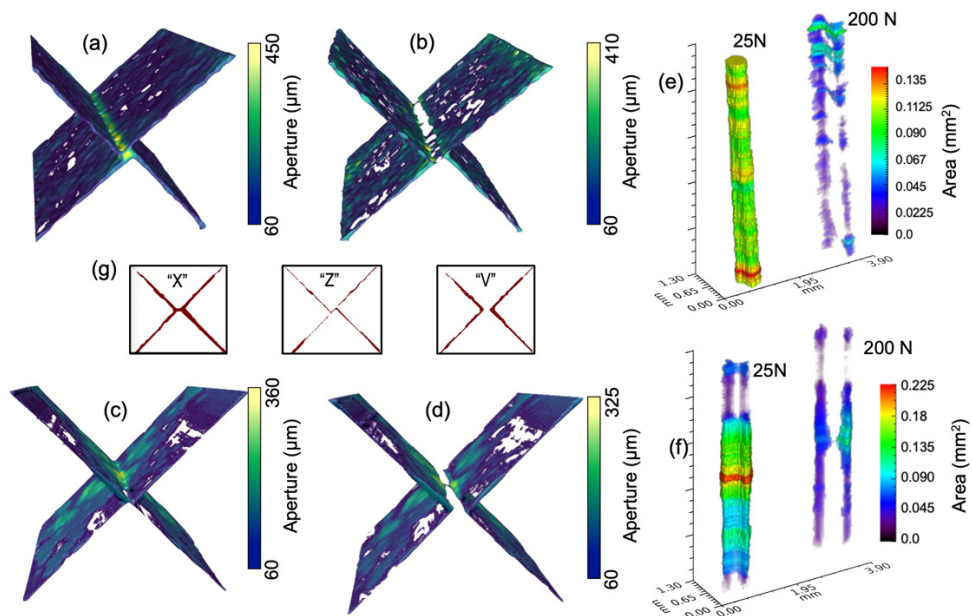

Figure 3. 3D reconstruction of the apertures for the "x" fracture networks with (a&b) random distribution of apertures under (a) 25 N and (b) 200 N, and with (c&d) a spatially correlated aperture distribution under (c) 25 N and (d) 200 N. The geometry of the intersection for loads 25 N and 200 N for the (e) random and (f) spatially correlated aperture distributions. (g) 2D images of illustrating the "X", Z" and "V" topology that can occur along a fracture intersection.

When the network was rotated to the "x" orientation relative to the applied normal load, the void volume and connectivity between the two fractures decreased significantly and, in some locations, ceased to exist at the highest load. The topology of the "x" orientation transitioned from "X" at 25 N to "Z" or "V" by 200 N (Figure 3g). In Figure 3e, the "Z" topology is observed in regions that are

still connected across the intersection. A "Z" topology can arise when there is shear offset at the intersection (Figure 3g). When the fractures are no longer connected across the intersection the network transitions to a "V" and two intersections are formed that result in two nearly linear flow paths (Figure 3e&f).

A comparison of the intersection geometry for the "+" and "x" orientations show that the spatial correlations in the aperture distribution affect the intersection geometry. Figures 2(e&f) and 3(e&f) show the extracted 3D intersection geometry from the networks with color representing the cross-sectional area of the intersection at that location. For the "+" orientation, the number and location of the necks (smallest cross-sectional area) along the intersection are affected by the spatial correlations in the aperture distribution. The necks occur preferentially near small apertures or regions of contacts in the horizontal fracture (Figure 2a-d). The necks remain open even at 200 N because the vertical fracture did not close or deform significantly. The mean eccentricity of the "+" intersection increased from roughly 0.6 to 0.75 as the load increased, while for the uncorrelated aperture distribution it increased from 0.45 to 0.6.

For the "x" orientation (Figure 3), as the topology changed from "X" to "Z" to "V", the intersection is observed to split into two parallel channels with necks that depend on the spatial correlations. For the uncorrelated "x" orientation (Figure 3e), the mean area decreased with increasing load while the mean eccentricity increased from 0.55 to 0.83, indicating that the intersection is essentially elongating preferentially in one direction. While the mean area also decreases with stress for the correlated "x" orientation (Figure 3f), the mean eccentricity ranged between $0.75 - 0.80$ for all loads. Figure 4 shows the probabilistic distributions of cross-sectional area along the intersection for both the "+" and "x" orientations. For the "+" orientation, the distributions (Figure 4a&c) did not change significantly with stress because only the horizontal fracture closed. In the "x' orientation where the fractures are subjected to both normal and shear stresses, a dramatic decrease in intersectional area is observed as the load increased from 25 N to 200 N. Also noted at 200N is the emergence of intersection cross-sections with areas larger than those observed at 25N. The increase in intersection area with stress occurs when there is a shear offset at the intersection at the onset of the transition to a "Z" topology at points along the intersection.
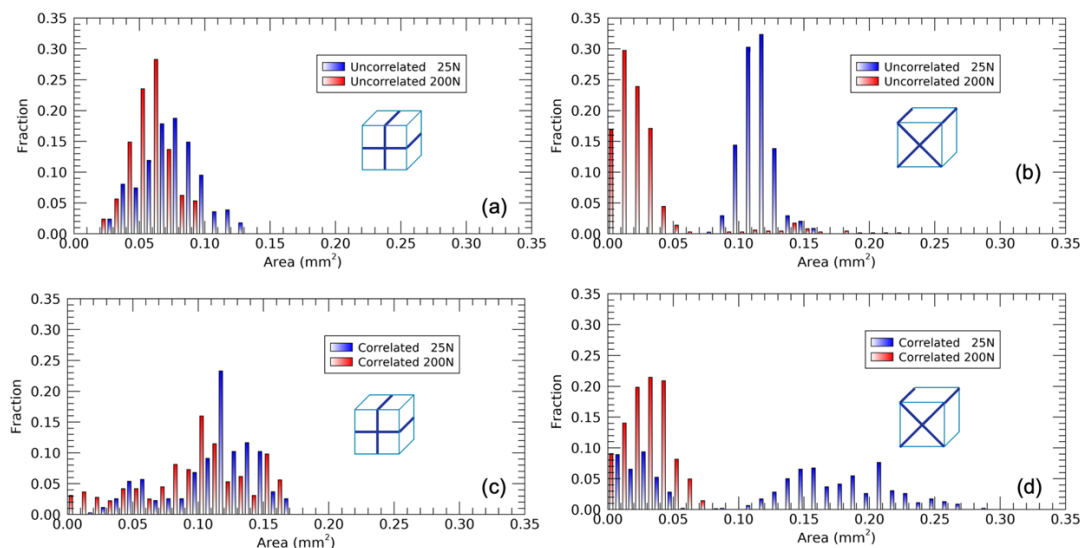

Figure 4. Probabilistic distribution of intersection cross-sectional area for the "+" (a&c) and "x" (b&d) fracture networks with (a & b) uncorrelated and (c &d) spatially correlated aperture distributions.

4   CONCLUSIONS

Though intersections compose only a tiny fraction of the total void volume of a fracture network, closure or opening of along an intersection can radically affect the flow paths through the network. The results of our experiments show that the orientation of a network relative to an applied stress

field controls the connectivity of the network and can change the topology of the fracture network and the geometry of the fracture intersections. The details of the spatial correlations in the aperture distributions along the individual fracture planes also affect the maintenance of connectivity as a network is stressed. For the same applied loads, a fracture network with a random distribution of apertures exhibited more connections between the two fractures than for the spatially correlated case. Just as for single fractures, networks with spatially correlated aperture distributions are dominated by only 1 or 2 flow paths that close more rapidly under stress than networks with random aperture distributions that can support multiple flow paths as stress is increased. These findings suggest that hydro-mechanical modeling of fracture networks for estimating or predicting reservoir performance should carefully consider how fracture network topology might evolve or be perturbed from changes in stress caused by engineering activities.

ACKNOWLEDGEMENTS

REFERENCES

Bai, T. X., Pollard, D. D., and Gao, H. (2000). Explanation for fracture spacing in layered materials. *Nature*, 403:753-756.

Cook, N.G., (1992) May. Natural joints in rock: mechanical, hydraulic, and seismic behaviour and properties under normal stress. In *International Journal of Rock Mechanics and Mining Sciences & Geomechanics Abstracts* (Vol. 29, No. 3, pp. 198-223). Pergamon.

Frash, L. P., Carey, J. W., Lei, Z., Rougier, E., Ickes, T., and Viswanathan, H. S. (2016). High-stress triaxial direct-shear fracturing of Utica shale and in situ x-ray microtomography with permeability measurement. *Journal of Geophysical Research*, 121:5493-5508. doi: https://doi.org/10.1002/2016JB012850

Hu, M. and Rutqvist, J. (2020). Microscale mechanical modeling of deformable geomaterials with dynamic contacts based on the numerical manifold method. *Computational Geosciences*, 24:1783–1797.

Hull, L. C., and Koslow, K. N. (1986). Streamline routing through fracture junctions. *Water Resources Research*, 22 (12):1731-1734.

Johnson, J. and Brown, S. (2001). Experimental mixing variability in intersecting natural fractures. *Geophysical Research Letters*, 28 (22):4303-4306.

Johnson, J., Brown, S., and Stockman, H. (2006). Fluid flow and mixing in rough-walled fracture intersections. *Journal of Geophysical Research-Solid Earth*, 111:(B12), 16.

Laubach, S. E., Lander, R. H., Criscenti, L. J., Anovitz, L. M., Urai, J., Pollyead, R., Hooker, J. N., Narr, W., Evans, M. A., Kerisit, S. N., Olson, J. E., Dewers, T., Fisher, D., Bodnar, R., Evans, B., Dove, P., Bonnell, L. M., Marder, M. P., Pyrak-Nolte, L. (2019). The role of chemistry in fracture pattern development and opportunities to advance interpretations of geological materials. *Reviews of Geophysics*, 57 (3):1065-1111.

Montemagno, C. D., Pyrak-Nolte, L. J. (1999). Fracture network versus single fractures: Measurement of fracture geometry with X-ray tomography. *Physics and Chemistry of the Earth Part a-Solid Earth and Geodesy*, 24(7):575-579.

Nolte, D. D. and Pyrak-Nolte, L. J. (1991). Stratified continuum percolation - scaling geometry of hierarchical cascades. *Phys. Rev. A.* 44:6320–6333.

Pyrak-Nolte, L. J., Nolte, D. D. (2016). Approaching a universal scaling relationship between fracture stiffness and fluid flow. *Nature Communications*, 7, Article Number 10663

Santos, A., Hu, M. and L. J. Pyrak-Nolte, Exploring the Geometry of Fracture Intersections under Stress, ARMA 22-637, *Proceedings of the 56th US Rock Mechanics / Geomechanics Symposium*, American Rock Mechanics Association, Santa Fe, New Mexico, June, 2022

Sanderson, D. J., Nixon, C. W. (2015). The use of topology in fracture network characterization. *Journal Of Structural Geology*, 72:55-66.